AIAA JOURNAL
Vol. 46, No. 11, November 2008

Surface Potential and Longitudinal Electric Field Measurements in the Aerodynamic Plasma Actuator

C. L. Enloe,* G. I. Font,† T. E. McLaughlin,‡ and D. M. Orlov§
United States Air Force Academy, Colorado 80840

DOI: 10.2514/1.33973

We present the results of a series of measurements in which an array of capacitive V-dot probes are used to determine the surface potential in a single dielectric barrier discharge plasma operated as an aerodynamic plasma actuator. From these measurements, we determine the longitudinal electric field in the plasma. The results show that the surface immediately (within the first alternating current cycle of the plasma discharge) acquires a net positive surface charge, so that the electric field in the plasma is asymmetric, the magnitude of the maximum field being more than 50% larger in the negative than the positive polarity. The measurements also show that there is a region several millimeters downstream from the exposed electrode edge over which the electric field maintains a constant positive (downstream) polarity over the course of the discharge cycle.

I. Introduction

THE single dielectric barrier aerodynamic plasma actuator is a dielectric barrier discharge (DBD) [1–15] in which an asymmetric arrangement of electrodes (one exposed, one encapsulated) produces a surface-mode discharge over the surface of the dielectric, leading to momentum coupling into neutral air [16–24]. As an aerodynamic flow-control device, the plasma actuator combines the desirable attributes of large control authority, high bandwidth, electrical efficiency, and simplicity of construction (no moving parts) applicable to aerodynamic flow control [25–47], including such specialized applications as flow control in turbines [48–52] and even flight control of entire aircraft [53–56]. The actuator has attracted the attention of a growing community of investigators. A substantial number of theoretical and numerical studies have been undertaken [57–65] in an attempt to describe the physics of the discharge itself, the understanding of which is a prerequisite to optimizing the actuator's effectiveness and efficiency. In some cases, the results of these studies are complementary. In others, the results contradict each other. Anchoring these results in experimental measurements has been difficult given the small scale size and transient nature of the DBD discharge, although efforts continue using novel experimental techniques [66–68].

In this paper, we present the results of an experiment designed to measure the surface potential of the dielectric as a function of space and time, from which the electric field in the plasma can be determined. Our experiment adapts the technique, common in the pulsed-power community, of using a capacitive V-dot probe [69] as a nonintrusive method of measuring time-varying electrical potentials. The chief difference between the traditional use of this probe and the one presented here is that we analyze the results to give us the potential at a location in between two conducting electrodes; namely, on the surface of the dielectric. We have shown in previous work [20] that acceleration of the neutral air occurs in a very thin region above the surface of the dielectric. Thus, the limitation of the technique we use here to one dimension along the dielectric surface is not a detriment to its usefulness in describing the physics of the DBD discharge.

II. Experimental Setup

Although a considerable body of work exists describing the discharge characteristics of the single dielectric barrier DBD, it is useful to facilitate an understanding of the present results by reviewing the fundamentals of the DBD's operation. The asymmetric arrangement of the electrodes in the plasma actuator is illustrated schematically in Fig. 1. In the plasma actuator, as in any DBD, there is no dc electrical path. Driven by a high ac applied voltage, the plasma exists as a series of microdischarges on the timescale of tens of nanoseconds [1,2,4–7,11,13–15], occurring between the exposed electrode and the dielectric surface. Because these microdischarges deposit charge on the dielectric surface that tends to reduce the applied electric field at that location, the plasma is self-limiting, and the microdischarge events naturally spread relatively uniformly along the length of the electrodes.

Consistent with our previous work [16,17], we define the "forward stroke" of the discharge as the discharge that develops when the exposed electrode is being driven to increasingly negative voltages, so that electrons are emitted from the exposed electrode and land on the dielectric surface. In contrast, the "backward stroke" occurs when the exposed electrode is driven to increasingly more positive voltages, so that electrons return from the dielectric surface to the exposed electrode. We have shown [1] that each of these portions of the discharge proceeds in three well-defined steps: ignition, expansion (during which the envelope of the discharge expands over the dielectric surface), and quenching (when the change in the voltage applied to the exposed electrode is no longer sufficient to maintain the discharge, given the buildup of relatively immobile charge on the dielectric surface). The results of the present experiment are consistent with this picture of the plasma's development.

A. Structure and Analysis of the V-Dot Probe

Implementing an array of V-dot probes to analyze the actuator's behavior is fairly straightforward. Each probe consists of a segmented portion of the encapsulated electrode that is electrically isolated from the remainder of the electrode. This segmented portion is then connected to the input of an op-amp-based active integrator, as shown in Fig. 2. Overall, the encapsulated electrode is the ground point of the plasma actuator circuit. Because of the op-amp's keeping both its inputs at the same potential, each isolated probe segment is also held at ground potential (less the IR voltage drop across the resistor R_{int}, which is trivial; in practice, we often let $R_{\text{int}} = 0$), so that

Received 13 August 2007; revision received 6 March 2008; accepted for publication 24 May 2008.

*Professor, Department of Physics. Senior Member AIAA.
†Professor, Department of Physics. Member AIAA.
‡Director, Aeronautics Research Center, Department of Aeronautics. Associate Fellow AIAA.
§Research Associate, Department of Physics. Member AIAA.

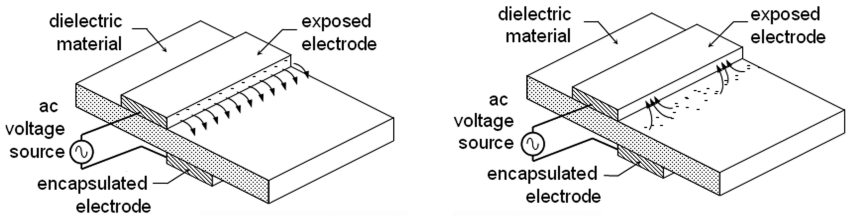

Fig. 1 Schematic representation of the "surface-mode" dielectric barrier discharge that comprises the aerodynamic plasma actuator.

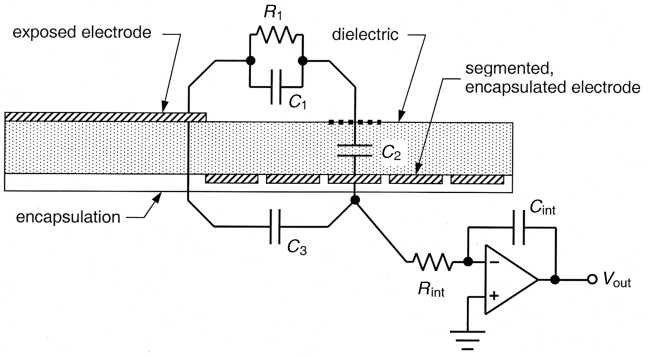

Fig. 2 Schematic representation of the V-dot probe used to determine surface potential on the plasma actuator.

the introduction of the probe does not perturb the normal functioning of the actuator.

Our experimental setup uses an array of 12 V-dot probes at evenly spaced locations downstream of the edge of the exposed electrode. The segments comprising the probes are 2.5 mm × 5 cm, staggered (as shown in Fig. 3), so that we have 1.25-mm resolution in the "chordwise" direction. The potential of the exposed electrode itself, measured by a commercial high-voltage oscilloscope probe, provides a 13th data point in our knowledge of the spatial variation in the surface potential.

To properly analyze the probe data, it is necessary to understand that the plasma actuator introduces both reactive and dissipative elements to the circuit of which it is a part. The dissipative element is the plasma itself, which exists only when the plasma ignites. (Depending on the temporal shape of the applied waveform, the duty cycle of the plasma can be a few percent up to 80–90% of the ac cycle. For the work shown here, we use a sinusoidal input waveform, and the plasma is ignited for approximately 50% of the time.) The reactive elements are the various capacitances formed by the actuator. These elements are shown schematically in Fig. 2, where we focus on a single one of the multiple V-dot probes.

We may consider the electric fields in the plasma actuator as originating on the exposed electrode and terminating on the encapsulated electrode, including on the isolated segments forming the V-dot probes. Some field lines pass through the dielectric material from below. This volume of the actuator forms the capacitance C_3 shown in Fig. 2. Because the lower electrode is encapsulated, no plasma forms there. Although the displacement currents flowing through C_3 are accounted for in the probe calibration, they simply comprise a reactive load on the ac power supply driving the actuator, and are not of primary interest in the functioning of the device. In contrast, it is the electric field originating above the dielectric surface that drives the formation of the DBD plasma. When the plasma forms, it comprises a resistive path from the exposed electrode to the surface of the dielectric. This conventional current, however, cannot penetrate the dielectric. Therefore, for purposes of analysis, we break this volume into two capacitances: C_1 is the capacitance between the exposed electrode and the dielectric surface, and C_2 is the capacitance between the dielectric surface and the encapsulated electrode.

When we operate the actuator at low voltages, below the breakdown threshold of the air, we still get a signal on each of the V-dot probes, because applying a voltage to the actuator charges the capacitance C_3 and the series capacitance C_1 and C_2, resulting in a displacement current which the integrator collects. This measurement comprises the first calibration of the probes. We find that the amplitude of the response of each of the probes to an applied voltage waveform is linear with the applied voltage amplitude to within ±1.5%, as shown in Fig. 4a for the case of a 2.1-mm-thick Macor dielectric ($\varepsilon_r = 6$). The largest displacement current, of course, flows to the probe nearest the electrode edge, as shown in Fig. 4b, so that the first calibration factor K_1 varies from $K_1 = 0.310$ V/kV for the probe nearest the edge to $K_1 = 0.008$ V/kV for the farthest-removed probe, for this particular material and geometry. It is necessary to do this calibration of the probes because this portion of the signal is always present, but it does not correspond to charging of the dielectric surface; rather, it represents the charging of the bulk actuator capacitance. Essentially, it corresponds to the boundary condition on the plasma that we already know from the direct measurement of the exposed electrode potential.

When applied voltage is such that the air breaks down, current flows through the plasma (resistor R_1) and *separately* charges the capacitance C_2, providing an *additional* displacement current input to the integrator. We determine the V-dot probes' response to this separate charging by temporarily extending the exposed electrode to

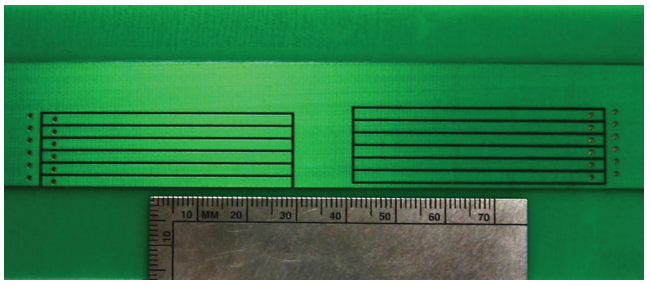

Fig. 3 Staggered, segmented electrodes afford 1.25-mm resolution measurements of the charge state of the dielectric surface.

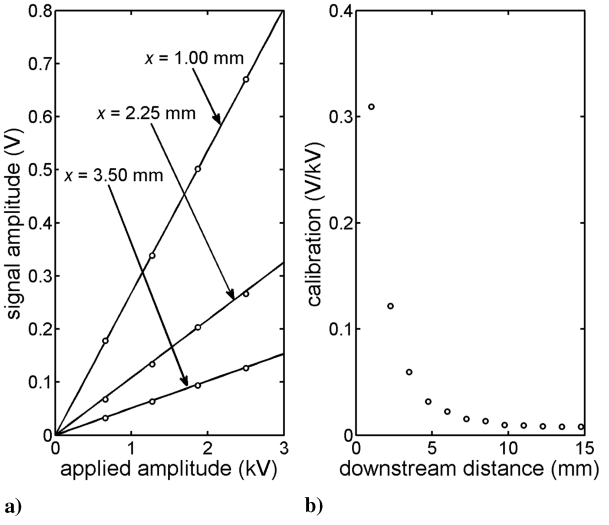

Fig. 4 Response of the V-dot probes to charging of the actuator's bulk capacitance.

cover the dielectric surface (a wide strip of copper tape is sufficient) and performing a second calibration of each of the probes. The result is a calibration factor that relates the probe voltage to the surface potential that is due to charge accumulation on the surface. Because the area of each of the probes is the same, and because the distance to the dielectric surface is the same for each, we would expect to find the same second calibration factor K_2 for each probe and, in fact, we do, to within $\pm 1.5\%$ ($K_2 = 0.296$ V/kV for the material and geometry at hand).

Whereas the first calibration factor is related wholly to the boundary condition at the exposed electrode, the portion of the V-dot probe signal to which the second calibration factor applies does not by itself reveal the total potential at the boundary of the plasma that is the dielectric surface. This is because, even in the absence of the plasma, the potential applied to the exposed electrode is divided by the series capacitance C_1 and C_2, and, in particular, is modified by the polarization charge that appears on the dielectric surface. It is this potential that is further modified by the accumulation of charge on the surface of the dielectric if the plasma forms in the gap. Fortunately, the capacitive division of the applied potential, and the influence of the polarization charge, is readily calculated from a solution to Laplace's equation, with appropriate boundary conditions. This results in a final dimensionless factor K_3, which varies from $K_3 = 1$ at the electrode edge to $K_3 \approx 0$ far from the exposed electrode. Given the signal from the ith probe $V_{\text{probe},i}(t)$, then, the potential $V_{\text{surf},i}(t)$, due to the accumulated physical charge on the surface at the probe location, is found by subtracting the contribution to the signal of the applied ac waveform $V_{\text{ac}}(t)$ and applying the appropriate calibration factor to the remaining probe response:

$$V_{\text{surf},i}(t) = \frac{V_{\text{probe},i}(t) - K_{1,i} V_{\text{ac}}(t)}{K_2} \tag{1}$$

The total surface potential $V_{\text{net},i}(t)$, then, including both the accumulated surface charge and the capacitive voltage division/polarization charge, is found from

$$V_{\text{net},i}(t) = V_{\text{surf},i}(t) + K_3 V_{\text{ac}}(t) \tag{2}$$

The amount of charge on the surface can be determined from the quantity V_{surf} because the capacitance C_2 can be readily calculated. The surface charge density σ is given by

$$\sigma = \left(\frac{\varepsilon_r \varepsilon_0}{d}\right) V_{\text{surf}} \tag{3}$$

where ε_0 is the permittivity of free space, ε_r is the relative dielectric constant of the dielectric material used in the actuator, and d is the thickness of the dielectric barrier.

As with many discharge phenomena, the uncertainty in the calibration of the probes is swamped by the variability in the repeatability of the data from shot to shot. For the data shown in this paper, one integrator circuit was switched among the 12 segments of the encapsulated electrode that comprised the V-dot probes; those segments that were not connected to the integrator were shorted to ground potential. Therefore, data showing the behavior of the actuator as a whole are amalgamated from multiple shots taken under identical conditions. We find that the repeatability in the dc component of surface charging that we observe is $\pm 7\%$ over the majority of the surface, rising to twice that value over the farthest-removed three probe channels. Similarly, the ac component of the surface charging (the amount of charge transferred per ac cycle) is repeatable to $\pm 4\%$ over the majority of the surface, again rising in the most remote three channels to twice this nominal value. These uncertainties are reflected in the appropriate plots later in this paper.

B. Sample V-Dot Probe Data

When the actuator is operating at normal voltage amplitudes, the output of a typical V-dot probe (after the integrator) looks like the trace shown in Fig. 5. The waveform is roughly sinusoidal (due to the integration of the displacement current from the bulk charging of the actuator's capacitance), but with deviations from a true sinusoidal shape (due to the effect of separately charging C_2 through the plasma). When we remove the effect of the former, by applying Eq. (1), the surface charging of the dielectric surface due to physical deposition of charges emerges. This charging is shown in Fig. 6, and is shown alongside a trace of the voltage applied across the electrodes of the actuator. The comparison between the two verifies the accuracy of the charging data. As mentioned previously, it has been well established that the actuator plasma quenches when, for a sinusoidal voltage waveform, the waveform reaches its extrema (times t_1 and t_3 shown in Fig. 6). Comparing the two traces in the figure, we see that the charging of the surface also stops changing at these times, so that the potential on the surface due to the charge accumulation remains constant until approximately one-quarter of the waveform's period later. At these points (times t_2 and t_4 in the figure), when the plasma ignites, we see that the potential on the dielectric surface begins to change rapidly due to the deposition (or removal) of physical charges on the surface. Therefore, our measurement of charge deposition is consistent with the well-established principles of operation of the dielectric barrier discharge.

Another obvious feature of the charging data is the immediate positive shift in the potential after the actuator is turned on. A comment on the use of an active integrator in the probe circuit is worthwhile at this point. An integrator has no dc response; rather, its

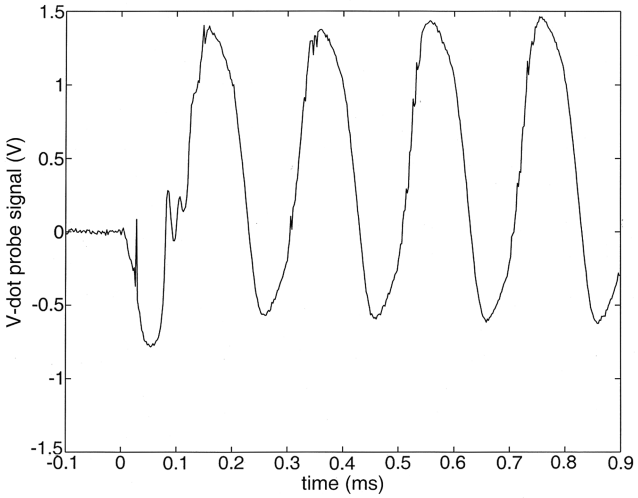

Fig. 5 Typical output signal from a V-dot probe with the plasma actuator in operation.

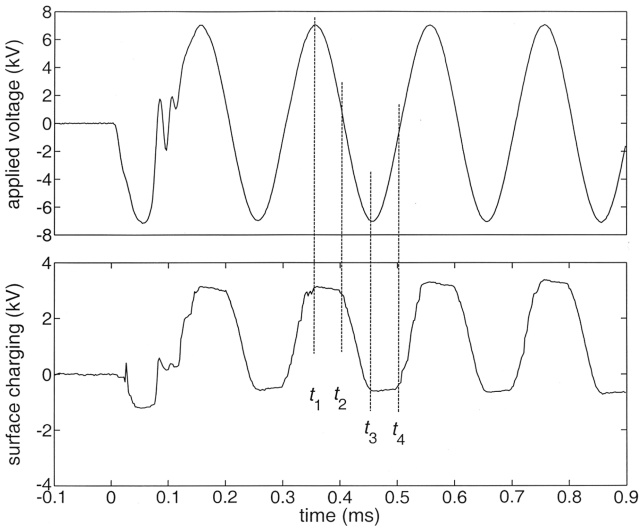

Fig. 6 Charging of the dielectric due to physical deposition of charges consistent with our knowledge of the ignition and quenching of the plasma.

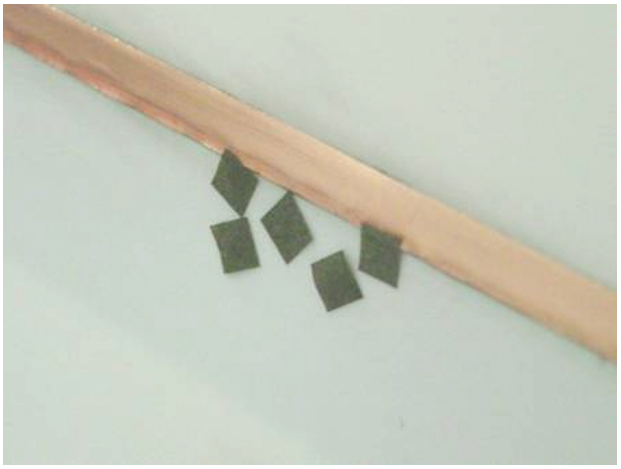

Fig. 7 Adhesion of tissue-paper squares to the dielectric surface indicates that dc charging of the surface is real and long-lived.

output is proportional to the time integral of the current charging the capacitor C_{int} in its feedback loop. It can detect a *change* in dc voltage levels on the dielectric surface if this change happens in a timescale shorter than the decay time for charge to dissipate from this capacitor. An ideal integrator holds charge on its capacitor C_{int} forever. This is not the case in an actual integrator circuit; neither would it be desirable could it be achieved. In practice, a large-value "bleed resistor" is placed across the capacitor to remove charge from the capacitor on long time scales. For our experiment, the decay time constant RC (resistance times capacitance) of the integrating circuit is 300 ms, versus the period of the applied ac high-voltage waveform, which varies from 0.2 to 8 ms in the data we show here. Therefore, all aspects of the integrator's output are valid, including the dc shift that happens within the first cycle of the applied ac waveform, given that we start from a known state of the actuator.

We find that the charging of the dielectric surface is extremely long-lived compared to the period of the applied ac waveform. Figure 7 shows a nonquantitative, yet important, measurement. After operating the actuator in a short burst, we note that lightweight tissue-paper squares stick to the vertical surface of the dielectric due to the surface charge there. The charge remains on the surface for many minutes. (Opaits et al. have tracked the decay of this dc surface charging and have found its lifetime to be on the order of tens of minutes [70].) Although the surface charge is long-lived, it is apparently not tightly bound to the surface. Wiping the surface with a solvent-soaked rag (we use acetone most commonly) removes the surface charge. Because the integrator will not respond to charge that is already present on the dielectric surface, for each of the measurements shown in this paper, we solvent-clean the dielectric surface before initiating the plasma. Thus, we start with a known, "clean" condition for each shot. Doing so, we note consistent results from shot to shot.

III. Experimental Results

We present here the surface potential and electric field as a function of longitudinal distance and time, determined by the V-dot probe technique described in the previous section, for a variety of typical aerodynamic plasma actuators. The actuators used in this experiment were all 22.5 cm in length, with the exposed (upper) electrode 0.65 cm in width, whereas the extent of the encapsulated (lower) electrode was 2.5 cm. We employed two different dielectric materials: Macor machinable ceramic with a relative dielectric constant of $\varepsilon_r = 6$, and a proprietary material with a relative dielectric constant of $\varepsilon_r = 3$. The thicknesses of these materials were comparable: $d = 2.1$ mm for the Macor, and $d = 1.5$ mm for the proprietary material. We also applied a thin (0.03 mm) layer of polyimide (Kapton) tape to the exposed surface of each of these dielectric materials to change the secondary electron emission properties without changing the bulk electric field structure in the actuator. The actuator was driven with a sinusoidal ac voltage, with an amplitude varying from 6.7 to 12.3 kV and a frequency varying from 125 Hz to 5 kHz.

A. Basic Surface Potential and Electric Field Measurements

All of the data shown here are from the first few ac cycles of the plasma, taken using a clean actuator; that is, the dielectric surface was cleaned with acetone before each data take. This allowed us to observe the charging of an initially uncharged dielectric surface with the V-dot probe diagnostic. Figure 8 shows the total surface potential as a function of space and time over the first four and one-half cycles of the plasma actuator's operation for the case of $V_{\text{ac}} = 6.7$ kV amplitude and $f = 5$ kHz. We see that the discharge settles very quickly (essentially, within one ac cycle) into a predictable pattern. In particular, the majority of the net positive charging of the dielectric surface is established by the end of the first positive-going half-cycle of the discharge. Figure 8 shows the total surface potential including all contributing factors. In Figs. 9 and 10, we distinguish between the total surface potential and that caused by the physical deposition of charge on the dielectric surface. Figure 9 shows surface charging for $x \approx d$. At this location, the contribution of the capacitive voltage division to the surface potential is substantial but by no means dominant. In Fig. 10, we have $x \approx 3d$. At this location, the deposition of physical charge on the surface dominates any other charging mechanism. We also note that the dc charging level at this location is large enough so that the surface potential never goes negative after the first ac cycle. For locations even farther from the electrode edge, the total surface potential and the surface potential due to surface charging alone are practically indistinguishable from each other. Although Fig. 8 is useful to present a bird's-eye view of the surface potential's behavior, it is much more beneficial to analyze these data by taking "slices" in space at various times during the discharge. These we present in Figs. 11–18 for four specific phases of the discharge's development discharge cycle. The times t_1–t_4 indicated in Figs. 11–18 correspond to the similarly labeled times in Fig. 8. At time t_1, the maximum positive excursion of the applied voltage, the plasma is quenched. At time t_2, the plasma is ignited for the forward stroke of the discharge. It quenches again at time t_3, the maximum negative excursion of the applied voltage, and ignites on the backward stoke at time t_4. At the moment the plasma quenches at the most positive excursion of the applied ac waveform, the surface potential across the entire dielectric surface is positive, as shown in Fig. 11. This figure follows the subsequent development of the surface potential between times t_1 and t_2. As the applied voltage becomes more negative, the surface potential follows, but only within approximately 5 mm (that is, two thicknesses of the dielectric) of the electrode edge. The potential is essentially unchanged over this time interval for distances 5 mm and farther from the electrode edge. The change in surface potential near the electrode edge is due to the capacitive voltage division in the circuit and the appearance of polarization charge on the surface of the dielectric. Figure 12 shows the longitudinal electric field values derived from the surface potential measurements. Note that there is a considerable portion of the surface over which the electric field is approximately constant, at a value of $E \approx 0.3$ MV/m.

The situation is qualitatively different once the plasma ignites at approximately $t = t_2$. Now, we see the effects (shown in Fig. 13) of negative charges being deposited on the dielectric surface as the plasma sweeps out away from the electrode [1,17]. There is still a region of net positive surface potential 5 mm and farther downstream from the electrode edge, and a region of positive electric field (shown in Fig. 14) a distance of 8 mm and farther from the edge, even at the maximum extent of this forward stroke discharge. Note that during this portion of the discharge, the largest magnitude of the longitudinal field is limited to a region approximately 2 mm from the edge of the exposed electrode. As the discharge extends over the surface, the electric field on the leading edge of the discharge is approximately one-third of that near the electrode.

There is a good deal of similarity between the behavior of the actuator between times t_3 and t_4 (shown in Figs. 15 and 16), when the plasma is again quenched [1,17], and the previous quenched phase

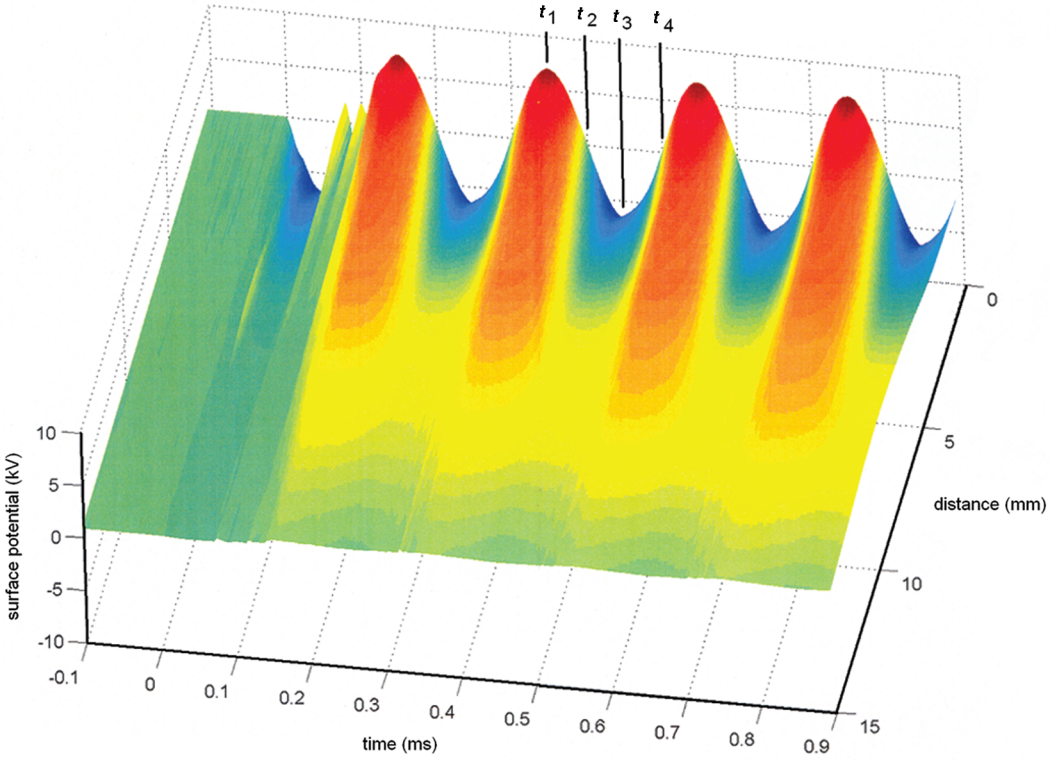

Fig. 8 Potential on the surface of the dielectric in the plasma actuator.

between times t_1 and t_2. As in the previous phase, again, we see that the surface potential and electric field 5 mm and farther downstream from the electrode edge are relatively unperturbed in the absence of a discharge; polarization charge effects are limited to the region nearest the exposed electrode.

The final phase of the discharge cycle, the ignition and expansion of the plasma in the backward stroke after time t_4 [1,17], is shown in Figs. 17 and 18. As the discharge sweeps over the surface, the positive surface potential noted at time t_1 is reestablished. Because the voltage waveform applied to the electrodes is symmetric, but the surface charge density is not, the maximum electric field in this phase of the discharge is less than in the forward stroke.

B. Other Determinations of Plasma Structure

Section III.A describes in detail the behavior of the dielectric barrier discharge for one set of discharge conditions. We performed similar analyses for different materials, frequencies, and amplitudes of the applied voltage waveform and obtained similar results. From the data, we can calculate several quantities of interest. One is the average value of the surface potential, which we find by simply taking an average over an integral number of ac cycles after the equilibrium has been established. These data are shown in Fig. 19, where we keep the applied voltage waveform constant at $V_{ac} = 6.7$ kV amplitude and $f = 5$ kHz, while changing the relative dielectric constant (and, to a lesser degree, the thickness) of the dielectric material. The figure shows that the surface charging extends over a larger extent of the dielectric surface. This is not unexpected, because the specific capacitance of the actuator with the lower dielectric constant is smaller, even accounting for the smaller thickness of the dielectric, requiring a smaller amount of surface charge to have the self-regulating effect that is the hallmark of the dielectric barrier discharge. We also note here that we see no

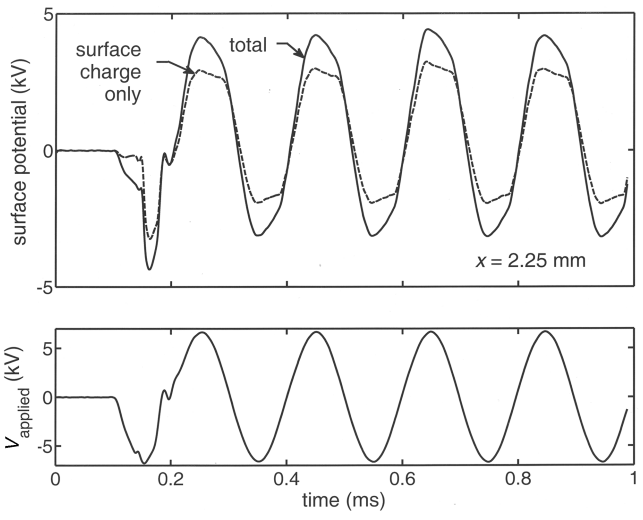

Fig. 9 Potential on the surface of the actuator's dielectric as a function of time at longitudinal distance $x = 2.25$ mm or $x \approx d$.

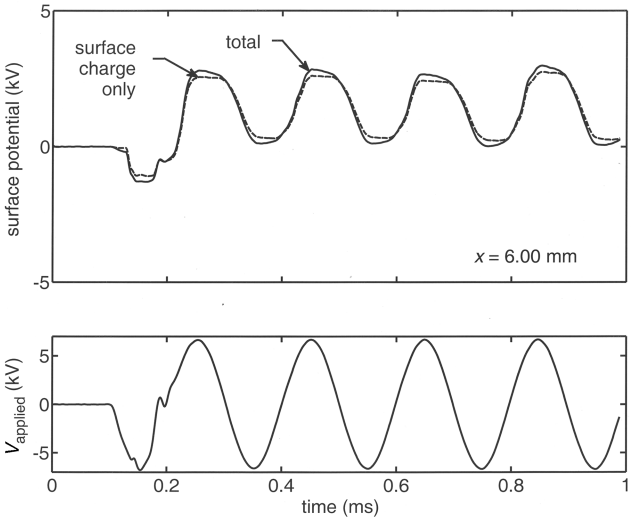

Fig. 10 Potential on the surface of the actuator's dielectric as a function of time at longitudinal distance $x = 6.00$ mm or $x \approx 3d$.

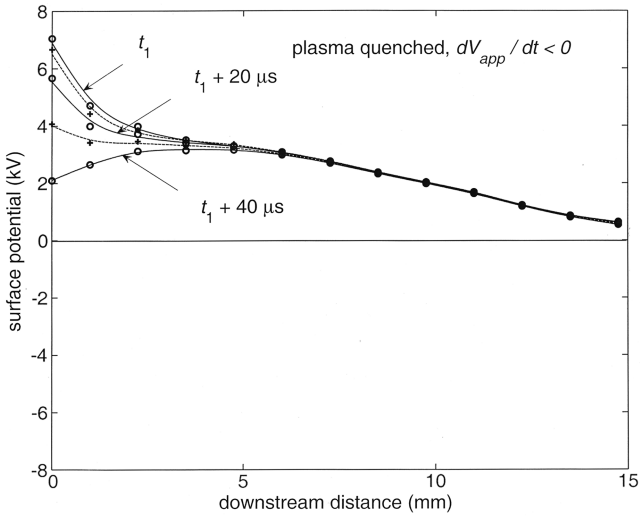

Fig. 11 Potential on the surface of the actuator's dielectric between times t_1 and t_2.

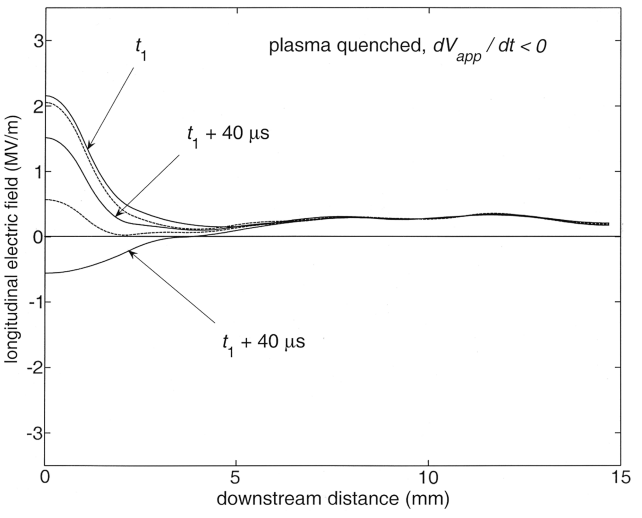

Fig. 12 Longitudinal electric field near the surface of the actuator's dielectric between times t_1 and t_2.

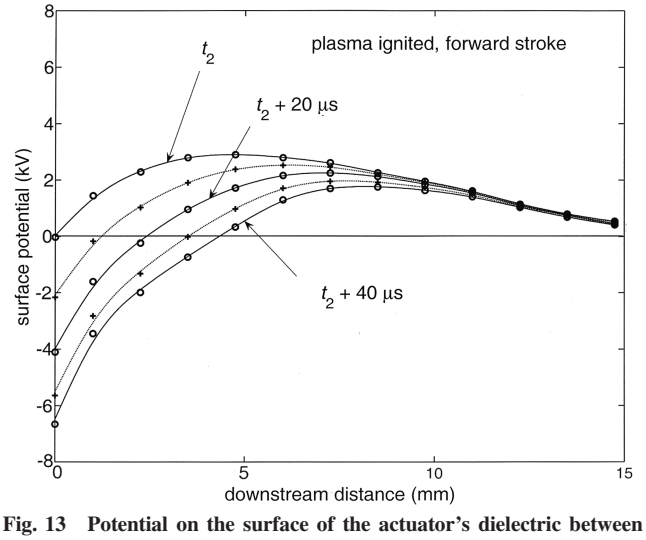

Fig. 13 Potential on the surface of the actuator's dielectric between times t_2 and t_3.

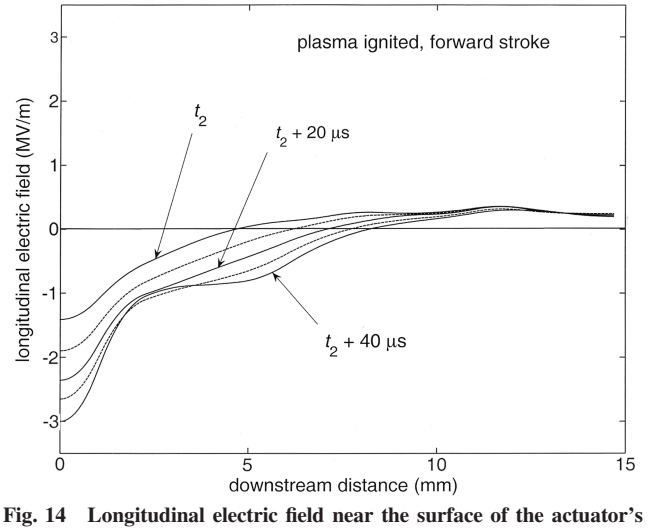

Fig. 14 Longitudinal electric field near the surface of the actuator's dielectric between times t_2 and t_3.

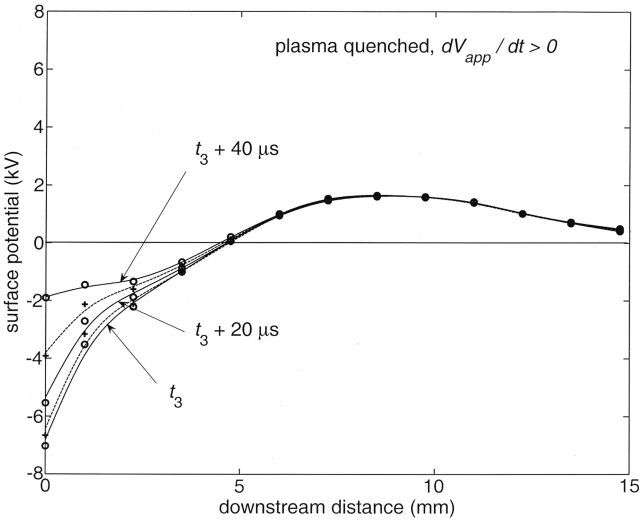

Fig. 15 Potential on the surface of the actuator's dielectric between times t_3 and t_4.

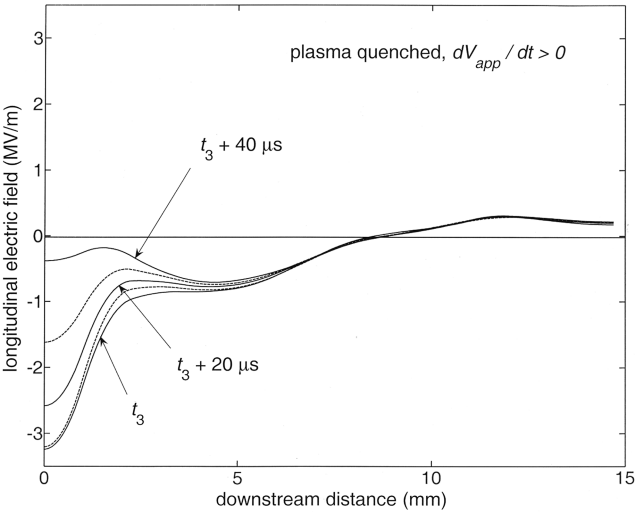

Fig. 16 Longitudinal electric field near the surface of the actuator's dielectric between times t_3 and t_4.

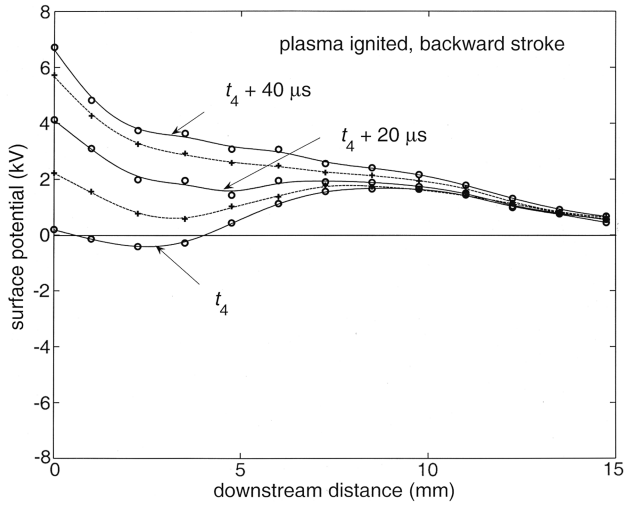

Fig. 17 Potential on the surface of the actuator's dielectric after time t_4.

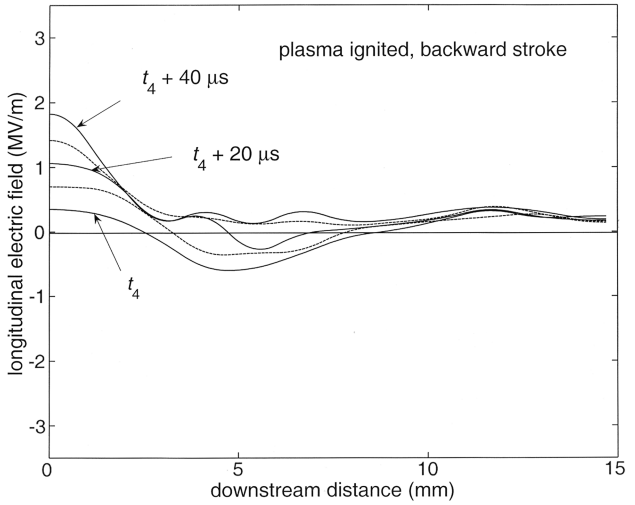

Fig. 18 Longitudinal electric field near the surface of the actuator's dielectric after time t_4.

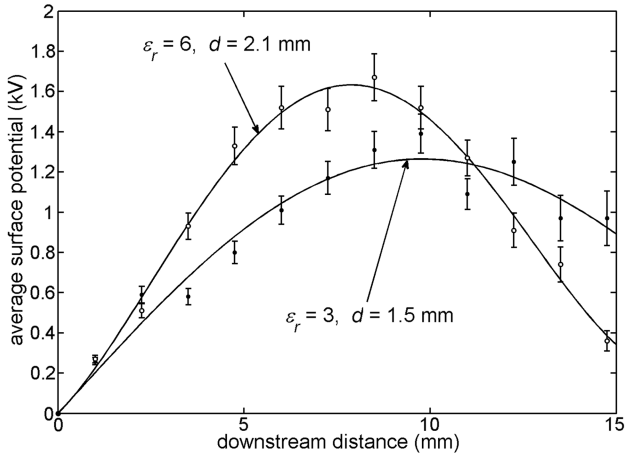

Fig. 19 Average surface potential on the dielectric as a function of distance for different dielectric materials.

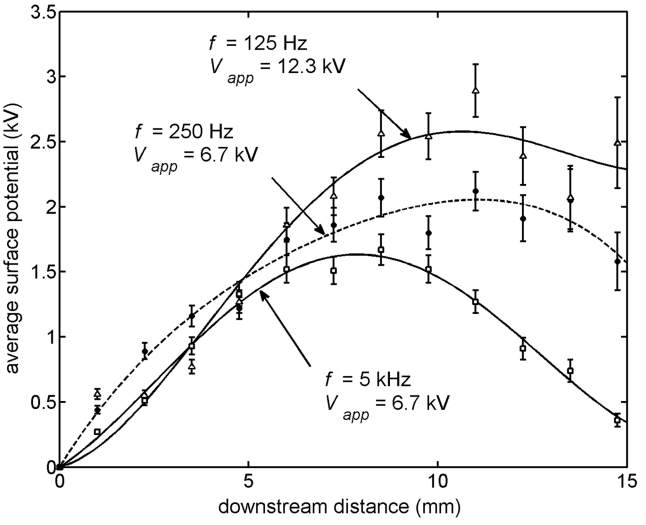

Fig. 20 Average surface potential on the dielectric as a function of distance for different applied voltage waveforms.

difference in the charge distribution when we change the surface properties (presumably including the secondary electron emission characteristics) by the addition of a thin polyimide layer. This implies that the spatial structure of the charge deposition is related primarily to the structure of the discharge and not to the characteristics of its dielectric boundary. When we keep the dielectric material properties the same (using the Macor dielectric $\varepsilon_r = 6$ and $d = 2.1$ mm), we obtain the results shown in Fig. 20, which are less intuitive to understand. Although it is not surprising that increasing the voltage amplitude of the applied waveform increases the surface charging, changing the frequency of the waveform independent of the amplitude also changes the charge distribution on the surface. In fact, it is the frequency of the applied waveform that seems to dictate the spatial variation in the surface charging, rather than the amplitude.

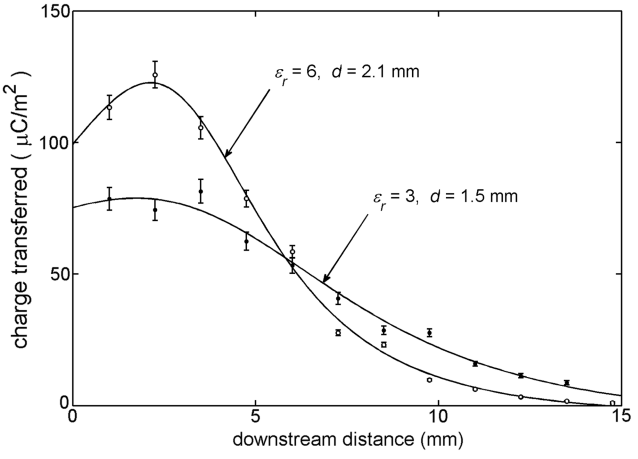

Fig. 21 Charge transferred per ac cycle as a function of location on the dielectric surface for different dielectric materials.

The ac variation in that portion of the surface potential that is due to the physical deposition of charge gives us the means to determine a quantity that relates directly to the structure of the discharge, namely, the charge transferred in each ac cycle as a function of the position x along the dielectric surface. Shown in Fig. 21, the results we obtain by changing the dielectric constant and thickness of the dielectric material are consistent with those shown in Fig. 19: the lower the specific capacitance, the more the discharge spreads over the surface of the dielectric. The most surprising result is shown in Fig. 22, where the structure of the discharge, as indicated by the spatial variation in the charge transferred, does not vary with frequency as long as the voltage amplitude is constant. Increasing the amplitude of the applied voltage, however, does change the structure of the discharge, not only increasing the magnitude of the charge transferred, but also the discharge's physical extent on the dielectric surface. This latter observation regarding the plasma's extent is consistent with measurements of the light emission from the plasma, which we have

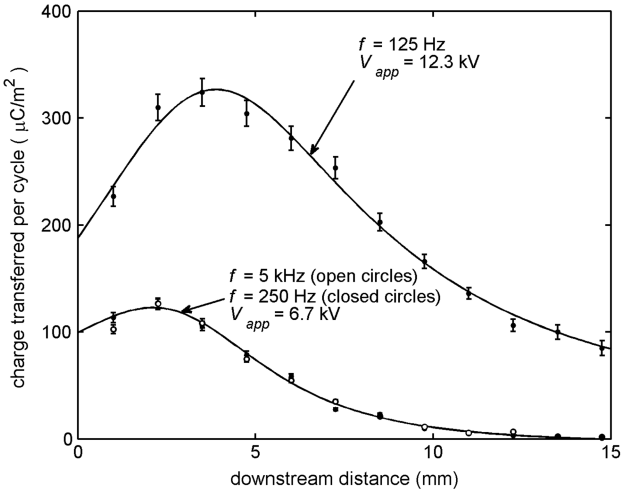

Fig. 22 Charge transferred per ac cycle as a function of location on the dielectric surface for different applied voltage waveforms.

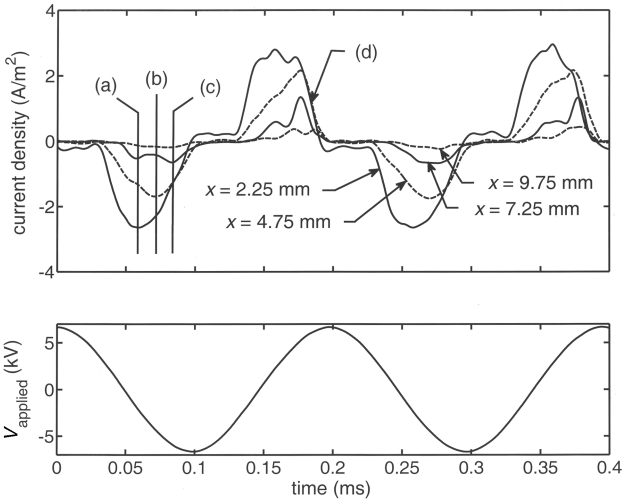

Fig. 23 Current density as a function of time for different locations on the dielectric surface.

seen from the earliest of our experiments with this type of discharge [17] and with what has been seen by others [67].

IV. Discussion

The dielectric barrier discharge plasma that comprises the aerodynamic plasma actuator is a physically small, transient plasma composed of multiple, overlapping microdischarge events. It is difficult to directly measure aspects of the plasma's development that bear directly on its effectiveness as an aerodynamic flow-control device. As with many in the community, our approach to understanding this plasma is to combine physical measurements with numerical modeling, allowing the measurements to validate the models and the models to guide the direction that our experimental investigations take. When we introduced the V-dot probe technique in a previous paper [71], it lacked sufficient resolution to generate data that could do much in the way of informing our view of the DBD plasma. Now, with the data from the array of probes that we present here, we can begin to see the signatures of different discharge structures on the "forward" and "backward" strokes of the discharge. In particular, Eq. (3) allows us to get information, resolved in both time and space, of the surface charging of the dielectric. Differentiating Eq. (3) in time for each of the probes allows us to determine the current density to the surface as a function of space and time. We present such information in Fig. 23, where we plot current density as a function of time to four downstream locations on the dielectric surface. Careful examination of the relative relationship of these traces yields insight into the plasma structure. For the negative-going portion of the discharge (the forward stroke), we see that the current to the surface peaks at the location of the nearest probe, at time a in the figure, before the peak occurs at time b at the farther downstream location, and that this peak likewise occurs before that at the farther downstream location, at time c. The behavior of the positive-going portion of the discharge (the backward stroke) is characteristically different. In this portion of the discharge, current to the nearest portion of the surface appears rapidly, whereas current to the farther locations increases roughly linearly with time. We see that the current to each location on the surface collapses rapidly at the same time, labeled d, (to within the time resolution of the probe) when the applied voltage reaches its extremum, and we know the discharge quenches.

This time and space profile of current deposition on the dielectric surface implies two different types of discharges in the forward and backward strokes. The description one takes away from the charge deposition in the negative-going case is one of a series of discharges that "leapfrog" each other as the overall discharge envelope expands over the dielectric surface with time. This progression is illustrated schematically in Fig. 24 and would result in the current to a particular location on the surface peaking earlier in time the closer that location is to the edge of the exposed electrode. In contrast, the current profile in the positive-going case implies a plasma in continuous contact with the surface, as would be the case were there streamers propagating across the surface, with subsequent streamers extending further across the surface as time progresses, as shown in Fig. 25. To support the idea that the discharge is characteristically different in the forward versus the backward strokes, we offer high-speed, image-intensified photographs of the discharge in each phase, shown in Fig. 26.

In our previous work [71], we did not yet appreciate the importance of the streamers in the backward stroke of the discharge. In that work, we simply did not carry out the simulation over a sufficiently long period of time to reveal the presence of the streamers. Our most recently published simulations [72] do show the streamer avalanche, and furthermore show that it is preceded by a

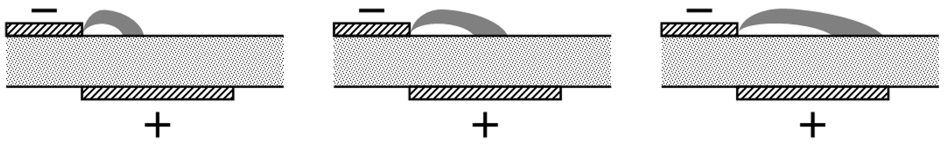

Fig. 24 Schematic description of the progress of the discharge in the negative-going or forward stroke of the DBD discharge.

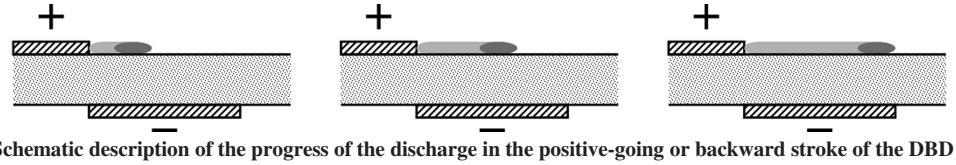

Fig. 25 Schematic description of the progress of the discharge in the positive-going or backward stroke of the DBD discharge.

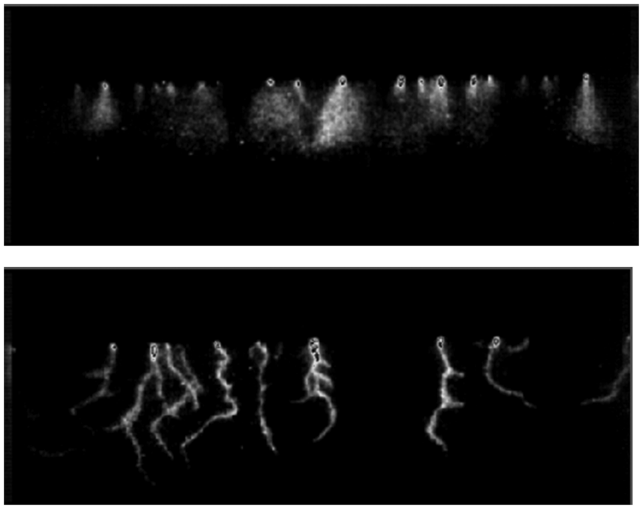

Fig. 26 High-speed photographs of the DBD discharge in the negative-going (forward) stroke (top) and the positive-going (backward) stroke (bottom).

relatively long period (hundreds of nanoseconds) where the discharge is in the glow phase. It is only after this charge buildup that the streamer appears.

In our previous work, from the results of our model of a single streamer, it was the positive-going or backward stroke that produced the majority of the force of the plasma actuator on the neutral air [71]. We have recently obtained direct, quantitative measurements, using optical interferometry, of the force applied by the actuator as a function of time [68], indicating clearly that the negative-going or forward stroke performs in excess of 95% of the momentum transfer to the neutral fluid. These results agree with those of Kim et al., who arrive at the same conclusion through an entirely different technique: phase-locked particle image velocimetry measurements [67]. With two unrelated measurement techniques giving the same result, the force production on the forward stroke must be considered to be a well-established phenomenon, at least for ac-driven plasmas. Also, we and others [18,67] have established the importance of the presence of oxygen in the air, and from this, presumably, the presence of negative oxygen ions in the plasma, to the force production of the DBD plasma actuator. Nonetheless, even our highest-fidelity simulations have yet to show the forward stroke's pushing the neutral fluid in the direction observed in the experiments. Any valid simulation of the actuator's operation must reproduce behavior that has been seen in multiple experiments. We strongly believe, based on work that is presently ongoing, that the key to understanding force production in the DBD plasma actuator lies in the interaction of multiple microdischarges, rather than the effect of an isolated discharge event.

At the very least, as the results presented here show, multiple discharge events over the ac cycle quickly establish an equilibrium charge condition on the dielectric surface. It would be highly unusual for two structurally different plasmas to be equally effective in depositing charge on the surface. In such a situation, we would expect that the surface would attain a dc charge state that would slow down the more efficient of the processes but enhance the less efficient of the two. We would infer, from the results presented here, that the streamer discharge on the backward (positive-going) stroke is the more effective of the two phases of the DBD discharge in depositing charge on the dielectric surface, probably by virtue of the plasma's longer contact time with the surface, because this would also be consistent with the marked effect of frequency of the ac cycle on the surface charge distribution (again, see Fig. 20).

Questions naturally arise as to whether the surface charging inherent in the DBD plasma actuator is beneficial or counterproductive in its effectiveness as a flow-control advice. At first blush, the presence of a persistent dc electric field pointing downstream, as Figs. 12, 14, 16, and 18 show, would seem to act against negative ions' accelerating neutrals in the downstream direction. Because the data we present here show how quickly the dc component of the surface charge develops, separating its effect is a difficult measurement to make. Nonetheless, we offer the results of a simple experiment with the proviso that it must be considered to be preliminary in its results. Placing the actuator (with the Macor dielectric) used in these experiments on our optical interferometry apparatus (described in [68]), we measure the force generated by the *first* negative-going pulse on the actuator with a clean (uncharged) dielectric surface, and compare that with a situation where we also observe the first negative-going pulse, but without cleaning the surface of charge beforehand. Our results indicate that a discharge across the positively charged surface produces considerably more force, by greater than a factor of 2, than a discharge across a clean (uncharged) surface. This could be because the discharge electric field is enhanced in the former case, but that is speculation at this point. It is just as likely that the presence of surface charge alters the discharge structure in a considerable way. Opaits et al. report that the presence of accumulated surface charge has a detrimental effect on the performance of their actuator [73], but their experiment was conducted for the case of short-pulse discharges in the presence of an applied dc electric field. Both experiments agree that dc surface charging is an important aspect of the surface-mode DBD discharge, one that directly impacts its effectiveness as a flow-control device, and one that certainly must be included in any theoretical or numerical description of the device.

V. Conclusions

The community's understanding of the surface-discharge-mode dielectric barrier discharge as an aerodynamic flow-control device is rapidly evolving. We claim as conclusions of this experiment only those phenomena that can be clearly seen in the data. Nonetheless, we have measured the charging of the dielectric surface in the single-dielectric-barrier-discharge plasma actuator, and, from this, have determined the longitudinal electric field and current density in the discharge, all as functions of time and longitudinal (spanwise) distance. We have shown that the surface immediately (within the first ac cycle of the applied voltage) develops a positive dc charge, around which the remainder of the discharge cycles oscillate. This level of surface charging can be a substantial fraction of the amplitude of the ac voltage applied to the actuator, and is spatially distributed with a peak downstream of the edge of the actuator's exposed electrode. Although the electric field near the edge of the electrode oscillates positive and negative, the electric field in the region downstream of the electrode assumes a single (positive; that is, in the downstream direction) polarity. Unlike the average charge distribution, the current density in the plasma peaks near the edge of the exposed electrode, in agreement with previous measurements of the light emission from the plasma. The extent of the surface charge distribution depends on the material properties (thickness and relative dielectric constant) of the dielectric material, as well as on the applied ac high-voltage waveform amplitude and frequency.

Acknowledgment

The authors gratefully acknowledge the support of the U.S. Air Force Office of Scientific Research, Rhett Jefferies, Program Manager, to the work presented here.

References

[1] Enloe, C. L., McLaughlin, T. E., VanDyken, R. D., and Fischer, J. R., "Plasma Structure in the Aerodynamic Plasma Actuator," AIAA Paper 2004-844, Jan. 2004.

[2] Kogelschatz, U., "Filamentary, Patterned, and Diffuse Barrier Discharges," *IEEE Transactions on Plasma Science*, Vol. 30, No. 4, 2002, pp. 1400–1408. doi:10.1109/TPS.2002.804201

[3] Haacke, M., Humpert, C., and Pietsch, G. J., "Influence of Field Strength and Energy Distribution of Different Barrier Discharge Arrangements on Ozone Generation," *Ozone Science and Engineering*, Vol. 24, No. 3, 2002, pp. 193–201. doi:10.1080/01919510208901610

[4] Mangolini, L., Orlov, K., Kortshagen, U., Heberlein, J., and

Kogelschatz, U., "Study of Different Discharge Regimes in a Dielectric Barrier Discharge: Electrical and Optical Characterization," *55th Annual Gaseous Electronics Conference*, American Physical Society Paper NR2.003, Oct. 2002.

[5] Kang, W. S., Kim, Y., and Hong, S. E., "Spatio-Temporal Images of Single Streamer Propagation in Dielectric Barrier Discharge," *IEEE Transactions on Plasma Science*, Vol. 30, No. 1, 2002, pp. 166–167. doi:10.1109/TPS.2002.1003976

[6] Napatovich, A. P., "Overview of Atmospheric Pressure Discharges Producing Nonthermal Plasmas," *Plasmas and Polymers*, Vol. 6, No. 1, 2001, pp. 1–14. doi:10.1023/A:1011313322430

[7] Gherardi, N., and Massines, F., "Mechanisms Controlling the Transition from Glow Silent Discharge to Streamer Discharge in Nitrogen," *IEEE Transactions on Plasma Science*, Vol. 29, No. 3, 2001, pp. 536–544. doi:10.1109/27.928953

[8] Liu, S., and Neiger, M., "Excitation of Dielectric Barrier Discharges by Unipolar Submicrosecond Square Pulses," *Journal of Physics D: Applied Physics*, Vol. 34, No. 11, 2001, pp. 1632–1638. doi:10.1088/0022-3727/34/11/312

[9] Kunhardt, E. E., "Generation of Large-Volume, Atmospheric-Pressure, Nonequilibrium Plasmas," *IEEE Transactions on Plasma Science*, Vol. 28, No. 1, 2000, pp. 189–200. doi:10.1109/27.842901

[10] Gibalov, V. I., and Pietsch, G. J., "The Development of Dielectric Barrier Discharges in Gas Gaps and on Surfaces," *Journal of Physics D: Applied Physics*, Vol. 33, No. 20, 2000, pp. 2618–2636. doi:10.1088/0022-3727/33/20/315

[11] Steinle, G., Neundorf, D., Hiller, W., and Pietralla, M., "Two-Dimensional Simulation of Filaments in Barrier Discharges," *Journal of Physics D: Applied Physics*, Vol. 32, No. 12, 1999, pp. 1350–1356. doi:10.1088/0022-3727/32/12/311

[12] Massines, F., Rabehi, A., Decomps, P., Ben Gadri, R., Segur, P., and Mayoux, C., "Experimental and Theoretical Study of a Glow Discharge at Atmospheric Pressure Controlled by Dielectric Barrier," *Journal of Applied Physics*, Vol. 83, No. 6, 1998, pp. 2950–2957. doi:10.1063/1.367051

[13] Xu, X., and Kushner, M. J., "Multiple Microdischarge Dynamics in Dielectric Barrier Discharges," *Journal of Applied Physics*, Vol. 84, No. 8, 1998, pp. 4153–4160. doi:10.1063/1.368629

[14] Li, J., and Dhali, S. K., "Simulation of Microdischarges in a Dielectric Barrier Discharge," *Journal of Applied Physics*, Vol. 82, No. 9, 1997, pp. 4205–4210. doi:10.1063/1.366223

[15] Falkenstein, Z., and Coogan, J. J., "Microdischarge Behavior in the Silent Discharge of Nitrogen-Oxygen and Water-Air Mixtures," *Journal of Physics D: Applied Physics*, Vol. 30, No. 5, 1997, pp. 817–825. doi:10.1088/0022-3727/30/5/015

[16] Enloe, C. L., McLaughlin, T. E., VanDyken, R. D., Kachner, K. D., Jumper, E. J., and Corke, T. C., "Mechanisms and Responses of a Single Dielectric Barrier Plasma Actuator: Plasma Morphology," *AIAA Journal*, Vol. 42, No. 3, 2004, pp. 589–594. doi:10.2514/1.2305

[17] Enloe, C. L., McLaughlin, T. E., VanDyken, R. D., Kachner, K. D., Jumper, E. J., Corke, T. C., Post, M., and Haddad, O., "Mechanisms and Responses of a Single Dielectric Barrier Plasma Actuator: Geometric Effects," *AIAA Journal*, Vol. 42, No. 3, 2004, pp. 595–604. doi:10.2514/1.3884

[18] Enloe, C. L., McLaughlin, T. E., Font, G. I., and Baughn, J. W., "Parameterization of Temporal Structure in the Single Dielectric Barrier Aerodynamic Plasma Actuator," *AIAA Journal*, Vol. 44, No. 6, June 2006, pp. 1127–1135. doi:10.2514/1.16297

[19] Gregory, J. W., Enloe, C. L., Font, G. I., and McLaughlin, T. E., "Force Production Mechanism of a Dielectric Barrier Discharge Plasma Actuator," AIAA Paper 2007-185, Jan. 2007.

[20] Enloe, C. L., McLaughlin, T. E., Font, G. I., and Baughn, J. W., "Frequency Effects on the Efficiency of the Aerodynamic Plasma Actuator," AIAA Paper 2006-166, Jan. 2006.

[21] Baughn, J. W., Porter, C. O., Peterson, B., McLaughlin, T. E., Enloe, C. L., Font, G. I., and Baird, C., "Momentum Transfer for an Aerodynamic Plasma Actuator with an Imposed Boundary Layer," AIAA Paper 2006-168, Jan. 2006.

[22] Porter, C., Baughn, J. W., McLaughlin, T. E., Enloe, C. L., and Font, G. I., "Temporal Force Measurements on an Aerodynamic Plasma Actuator," AIAA Paper 2006-104, Jan. 2006.

[23] Baird, C., Enloe, C. L., McLaughlin, T. E., Baughn, J. W., "Acoustic Testing of the Dielectric Barrier Discharge (DBD) Plasma Actuator," AIAA Paper 2005-0565, Jan. 2005.

[24] VanDyken, R. D., Enloe, C. L., and McLaughlin, T. E., "Parametric Investigations of Single Dielectric Barrier Plasma Actuator," AIAA Paper 2004-846, Jan. 2004.

[25] Porter, C. O., McLaughlin, T. E., Enloe, C. L., and Font, G. I., "Boundary Layer Control Using a DBD Plasma Actuator," AIAA Paper 2007-786, Jan. 2007.

[26] Orlov, D., Apker, T., He, C., Othman, H., and Corke, T., "Modeling and Experiment of Leading Edge Separation Control Using SDBD Plasma Actuators," AIAA Paper 2007-877, Jan. 2007.

[27] Ng, T., Patel, M., Vasudevan, S., Corke, T., Post, M., and McLaughlin, T. E., "Scaling Effects of an Aerodynamic Plasma Actuator," AIAA Paper 2007-635, 2007.

[28] Post, M., Greenwade, S., Yan, M., Corke, T., and Patel, M., "Effects of an Aerodynamic Plasma Actuator on a HSNLF Airfoil," AIAA Paper 2007-638, Jan. 2007.

[29] Bolitho, M., and Jacob, J., "Use of Aggregate Plasma Synthetic Jet Actuators for Flow Control," AIAA Paper 2007-637, Jan. 2007.

[30] Santhanakrishnan, A., and Jacob, J., "Formation and Scaling of Plasma Synthetic Jet Actuators," AIAA Paper 2007-940, Jan. 2007.

[31] Thomas, F., Kozlov, A., and Corke, T., "Plasma Actuators for Bluff Body Flow Control," AIAA Paper 2006-2845, June 2006.

[32] Santhanakrishnan, A., and Jacob, J., "Flow Control Using Plasma Actuators and Linear/Annular Plasma Synthetic Jet Actuators," AIAA Paper 2006-3033, June 2006.

[33] McLaughlin, T. E., Felker, B., Avery, J., and Enloe, C. L., "Further Experiments on Cylinder Wake Modification with Dielectric Barrier Discharge Forcing," AIAA Paper 2006-1409, Jan. 2006.

[34] Corke, T., Mertz, B., and Patel, M., "Plasma Flow Control Optimized Airfoil," AIAA Paper 2006-1208, Jan. 2006.

[35] Post, M., and Corke, T., "Overview of Plasma Flow Control: Concepts, Optimization, and Application," AIAA Paper 2005-0563, Jan. 2005.

[36] Hall, K., and Jumper, E., "Potential Flow Model of a Plasma Actuator as a Lift Enhancement Device," AIAA Paper 2005-0563, Jan. 2005.

[37] McLaughlin, T., Munska, M., Vaeth, J., Dauwalter, T., Goode, J., and Siegel, S., "Plasma-Based Actuators for Cylindrical Wake Vortex Control," AIAA Paper 2004-2129, June 2004.

[38] Corke, T., and He, C., "Plasma Flaps and Plasma Slats: An Application of Weakly-Ionized Plasma Actuators," AIAA Paper 2004-2127, June 2004.

[39] Post, M., and Corke, T., "Separation Control Using Plasma Actuators: Dynamic Stall Control on an Oscillating Airfoil," AIAA Paper 2004-2517, June 2004.

[40] Post, M., and Corke, T., "Separation Control Using Plasma Actuators: Stationary & Oscillating Airfoils," AIAA Paper 2004-841, Jan. 2004.

[41] Wilkinson, S., "Investigation of an Oscillating Surface Plasma for Turbulent Drag Reduction," AIAA Paper 2003-1023, Jan. 2003.

[42] Post, M., and Corke, T., "Separation Control on High Angle of Attack Airfoil Using Plasma Actuators," AIAA Paper 2003-1024, Jan. 2003.

[43] Ashpis, D., and Hultgren, L., "Demonstration of Separation Delay with Glow Discharge Plasma Actuators," AIAA Paper 2003-1025, Jan. 2003.

[44] Corke, T. C., Jumper, E. L., Post, M. L., Orlov, D., and McLaughlin, T. E., "Application of Weakly-Ionized Plasmas as Wing Flow-Control Devices," AIAA Paper 2002-0350, Jan. 2002.

[45] Roth, J. R., Sherman, D. M., and Wilkinson, S. P., "Electrohydrodynamic Flow Control with a Glow-Discharge Surface Plasma," *AIAA Journal*, Vol. 38, No. 7, 2000, pp. 1166–1172. doi:10.2514/2.1110

[46] Corke, T. C., and Matlis, E., "Phased Plasma Arrays for Unsteady Flow Control," AIAA Paper 2000-2323, Jan. 2000.

[47] Roth, J. R., Sherman, D. M., and Wilkinson, S. P., "Boundary Layer Flow Control with a One Atmosphere Uniform Glow Discharge Surface Plasma," AIAA Paper 98-0328, Jan. 1998.

[48] Van Ness, D., Corke, T., and Morris, S., "Stereo PIV of a Turbine Tip Clearance Flow with Plasma Actuation," AIAA Paper 2007-647, Jan. 2007.

[49] Douville, T., Stephens, J., Corke, T., and Morris, S., "Turbine Blade Tip Leakage Flow Control by Partial Squealer Tip and Plasma Actuators," AIAA Paper 2006-20, Jan. 2006.

[50] Morris, S., Corke, T., Van Ness, D., and Cameron, J., "Plasma Actuators for Tip Clearance Flow Control," AIAA Paper 2005-0782, Jan. 2005.

[51] List, J., Byerley, A., McLaughlin, T., and VanDyken, R., "Using Plasma Actuator Flaps to Control Laminar Separation on Turbine Blades in a Linear Cascade," AIAA Paper 2003-1026, Jan. 2003.

[52] Huang, J., Corke, T., and Thomas, F., "Plasma Actuators for Separation

Control of Low Pressure Turbine Blades," AIAA Paper 2003-1027, Jan. 2003.
[53] Lopera, J., Ng, T., Patel, M., Vasudevan, S., and Corke, T., "Aerodynamic Control of 1303 UAV Using Windward Surface Plasma Actuators on a Separation Ramp," AIAA Paper 2007-636, Jan. 2007.
[54] Patel, M., Ng, T., Vasudevan, S., Corke, T., and He, C., "Plasma Actuators for Hingeless Aerodynamic Control of an Unmanned Air Vehicle," AIAA Paper 2006-3495, June 2006.
[55] Patel, M., Sowle, Z., Corke, T., and He, C., "Autonomous Sensing and Control of Wing Stall Using a Smart Plasma Slat," AIAA Paper 2006-1207, Jan. 2006.
[56] Patel, M., Sowle, Z., Corke, T., and He, C., "Detection and Control of Wing Stall Using Plasma Actuators," AIAA Paper 2005-1233, Jan. 2005.
[57] Font, G. I., "Boundary Layer Control with Atmospheric Plasma Discharges," *AIAA Journal*, Vol. 44, No. 7, 2006, pp. 1572–1578. doi:10.2514/1.18542
[58] Boeuf, J. P., and Pitchford, L. C., "Electrohydrodynamic Force and Aerodynamic Flow Acceleration in Surface Dielectric Barrier Discharge," *Journal of Applied Physics*, Vol. 97, No. 10, 2005, p. 103307. doi:10.1063/1.1901841
[59] Roy, S., "Flow Actuation Using Radio Frequency in Partially Ionized Collisional Plasmas," *Applied Physics Letters*, Vol. 86, No. 10, 2005, p. 101502. doi:10.1063/1.1879097
[60] Likhanskii, A., Shneider, M., Opaits, D., Macheret, S., and Miles, R., "Numerical Modeling of DBD Plasma Actuators and the Induced Air Flow," AIAA Paper 2007-4533, June 2007.
[61] Likhanskii, A., Shneider, M., Macheret, S., and Miles, R., "Optimization of Dielectric Barrier Discharge Plasma Actuators at Atmospheric and Subatmospheric Pressures," AIAA Paper 2007-0633, Jan. 2007.
[62] Orlov, D. M., and Corke, T. C., "Numerical Simulation of Aerodynamic Plasma Actuator Effects," AIAA Paper 2005-1083, Jan. 2005.
[63] Font, G. I., and Morgan, W. L., "Plasma Discharges in Atmospheric Pressure Oxygen for Boundary Layer Separation Control," AIAA Paper 2005-4632, June 2005.
[64] Gaitonde, D. V., Visbal, M. R., and Roy, S., "Control of Flow past a Wing Section with Plasma-Based Body Forces," AIAA Paper 2005-5302, June 2005.
[65] Likhanskii, A. V., Semak, V. V., Shneider, M. N., Opaits, D. F., Miles, R. B., and Macheret, S. O., "Parallel Code Development and Numerical Investigation of Surface Charge Build-Up in DBD Actuators," AIAA Paper 2008-1380, Jan. 2008.
[66] Takizawa, Y., Matsuda, A., Kikuchi, K., Sasoh, A., and Takashi, A., "Optical Observations of Discharge Plasma Structure in DBD Plasma Actuator," AIAA Paper 2007-4376, June 2007.
[67] Kim, W., Do, H., Mungal, M. G., and Cappelli, M. A., "On the Role of Oxygen in Dielectric Barrier Discharge Actuation of Aerodynamic Flows," *Applied Physics Letters*, Vol. 91, No. 18, 2007, p. 181501. doi:10.1063/1.2803755
[68] Enloe, C. L., McHarg, M. G., and McLaughlin, T. E., "Time-Correlated Force Production Measurements of the Dielectric Barrier Discharge Plasma Aerodynamic Actuator," *Journal of Applied Physics*, Vol. 103, April 2008, p. 073302. doi:10.1063/1.2896590
[69] Humphries, S., *Principles of Charged Particle Acceleration*, Wiley, New York, 1986, pp. 275–276.
[70] Opaits, D. F., Neretti, G., Zaidi, S. H., Shneider, M. N., Miles, R. B., Likhanskii, A. V., and Macheret, S. O., "DBD Plasma Actuators Driven by a Combination of Low Frequency Bias Voltage and Nanosecond Pulses," AIAA Paper 2008-1372, Jan. 2008.
[71] Font, G. I., Enloe, C. L., McLaughlin, T. E., and Orlov, D. M., "Plasma Discharge Characteristics and Experimentally Determined Boundary Conditions for a Plasma Actuator," AIAA Paper 2007-0188, Jan. 2007.
[72] Orlov, D. M., Font, G. I., Enloe, and Edelstein, D., "Characterization of Discharge Modes of the Plasma Actuator," AIAA Paper 2008-1409, Jan. 2008.
[73] Opaits, D. F., Neretti, G., Likhanskii, A. V., Zaidi, S., Shneider, M. N., and Miles, R. B., "Experimental Investigation of DBD Plasma Actuators Driven by Repetitive High Voltage Nanosecond Pulses with DC or Low-Frequency Sinusoidal Bias," AIAA Paper 2007-4532, June 2007.

D. Gaitonde
Associate Editor